Pressure-Sensitive Supramolecular Adhesives Based on Lipoic Acid and Bio-friendly Dynamic Cyclodextrin and Polyrotaxane Cross-Linkers

Karan Vivek Dikshit,† Aseem Milind Visal,† Femke Janssen,‡ Alexander Larsen,¶ and Carson J. Bruns*,¶,§

†Materials Science and Engineering, University of Colorado Boulder, Boulder, CO, USA 80303

‡Chemical and Biological Engineering, University of Colorado Boulder, Boulder, CO, USA 80303

¶Paul M. Rady Department of Mechanical Engineering, University of Colorado Boulder, Boulder, CO, USA 80309

§ATLAS Institute, University of Colorado Boulder, Boulder, CO, USA 80309

E-mail: carson.bruns@colorado.edu

Keywords

biocompatible, supramolecular, host-guest, adhesives, soft materials, polyrotaxanes, cyclodextrin, slide-ring networks

Abstract

Slide-ring materials are polymer networks with mobile cross-links that exhibit impressive stress dissipation and fracture resistance owing to the pulley effect. On account of their remarkable ability to dissipate the energy of deformation, these materials have found their way into advanced materials such as abrasion-resistant coatings and elastic battery electrode binders. In this work, we explore the role of mobile cross-links on the properties of a bio-friendly pressure-sensitive adhesive made using composites of cyclodextrin-based macromolecules and poly(lipoic acid). We modify cyclodextrin-based hosts and polyrotaxanes with pendant groups of lipoic acid (a commonly ingested antioxidant) to incorporate them as cross-links in poly(lipoic acid) networks obtained by simple heating in open air. By systematically varying the adhesive formulations while probing their mechanical and adhesive properties, we uncover trends in structure-property relationships that enable one to tune network properties and access bio-friendly, high-tack adhesives.

Introduction

While supramolecular adhesives have been in development since adhesion enhancements due to self-assembly were first discovered in the 1990s, 1 research interest in these materials has surged in the past few years. $^{2-5}$ Noncovalent interactions such as hydrogen bonding, 6 ion pairing, 7 hydrophobic effects, 8 metal-ligand complexation, 9 and π - π stacking 10 adhere these materials to a wide variety of glass, ceramic, metal, plastic, and natural substrates. Supramolecular motifs may further confer a number of beneficial properties to adhesive materials, including the capacity for stimulus response, 11,12 self healing, 13 high strength, 14 or resistance to water 15 and other solvents. 16 Some prominent examples of supramolecular adhesives include mussel-inspired polymers functionalized with catechols 17 (which combine several types of interactions 18), self-complementary hydrogen bonding pairs such as nucleobases 19 and ureidopyrimidanones, 20 and a variety of macrocyclic host-guest systems. 21

Lipoic acid (LA), a natural product and dietary supplement consumed as an anti-oxidant, has recently been identified as a promising synthon for adhesives.²² The dithiolane moiety of LA undergoes ring-opening polymerization^{23–25} spontaneously in melt to form poly(LA) via disulfide exchange.²⁴ Rich in carboxylate groups, poly(LA) demonstrates excellent ad-

hesive properties, ^{26–28} but only if its tendency to crystallize ²⁹ is suppressed. Vinyl³⁰ and iron ^{22,31} additives are simple, low-cost options to hinder poly(LA) crystallinity via cross-linking, producing materials that are remarkably adhesive and extensible. Cyclic poly(LA) obtained by ring-opening polymerization ^{32,33} can also display suppressed crystallinity, good adhesion, and recyclability. ²⁶ The reversibility and redox sensitivity of the disulfide bonds in the poly(LA) backbone also imparts the adhesives with redox- and temperature-responsive behavior and the capacity for self-healing. ²²

Another promising motif for supramolecular adhesives is the bead-on-string structure of polyrotaxanes (PRs).³⁴ The translation of macrocycles along a PR backbone provides an additional mechanism for stress dissipation beyond chain uncoiling and stretching.^{35,36} PRs have been used in a number of adhesive formulations to bond materials such as hydrogels,^{37,38} organogels,³⁹ resins,⁴⁰ and cells.^{41,42} PRs have also demonstrated remarkable performance as adhesive binders in Si-anode batteries,⁴³⁻⁴⁵ attributed to their ability to dissipate the large stresses associated with volumetric changes at the anode. Recently, acrylic-based pressure-sensitive adhesives derived from PRs have been reported to exhibit high adhesive energies and large extensibilities attributable to ring sliding.⁴⁶ PRs are most commonly assembled from cyclodextrin (CD) hosts, since they are commercially available, bio-friendly, and capable of threading a variety of polymer chains.⁴⁷ However, hydrogen bonding among the CD rings imparts these PRs with low solubility^{48,49} and they char instead of melting,^{50,51} which precludes them from most conventional materials processing techniques.⁵² Therefore, CD-based PRs are typically functionalized to improve their processability and functionality.^{39,53,54}

Pressure-sensitive adhesives (PSAs) are viscoelastic polymers that quickly bond with various substrates under light applied pressure due to high fluidity, elasticity, and cohesive strength. ⁵⁵ The need for bio-based and bio-friendly adhesives is of great interest ^{56–58} because of the negative environmental impact of current petroleum-based adhesives. In this regard, poly(LA) and cyclodextrin-based compounds are both attractive because they are food-grade materials that can be sourced from renewable bio-based feedstocks. How-

ever, adhesives based on both of these polymers often compromise on sustainability through modification with petroleum-based acrylics $^{43-46}$ or vinyl 22 compounds. Here we introduce new supramolecular PSA materials derived from viscoelastic LA polymers cross-linked by bio-friendly cyclodextrin-based compounds in the form of lipoated α -cyclodextrin (LCD) or lipoated PEG \subset (α -CD)_n PRs (LPR). Adhesion of PSAs is strongly dominated (>99%) by the work of viscoelastic deformation during failure of the bond. Therefore, LPR is expected to to enhance energy dissipation (and therefore adhesive strength) by way of its ring-sliding motions, also known as the pulley effect, 53,59,60 under viscoelastic deformation. Since α -CD is known to host LA 61 and many alkanoic acids, 62 we also expect a binding interaction between LCD and the pentanoate side chains of poly(LA), and possibly even through-the-annulus threading during polymerization, 46 thus providing a similar mechanism for dissipating mechanical energy through dynamic host-guest exchange. Lipoated poly(vinyl alcohol) (LPVA) is included as a biocompatible, yet petroleum-based and non-supramolecular control. A widely available commercial PSA (UHU Tac) that claims strong adhesion to most surfaces is chosen as a petrochemical-derived adhesive for the sake of comparison.

Experimental section

Materials

35 kDa molecular weight (MW) poly(ethylene glycol) (PEG35k) was purchased from EMD Millipore Corporation. (2,2,6,6-tetramethylpiperidin-1-yl)oxyl (TEMPO) and 1-adamantanamine hydrochloride (AdNH₂·HCl) were purchased from TCI America. α -Cyclodextrin (α -CD), (benzotriazol-1-yloxytris(dimethylamino)phosphonium hexafluorophosphate) (BOP) reagent, and D,L- α -lipoic acid (LA) were purchased from Chem Impex International, Inc. Ethylene diisopropylamine (EDIPA) was purchased from Alfa Aesar. Carbonyldiimidazole (CDI) and sodium hypochlorite (NaOCl) solution with 5% free chlorine was purchased from Spectrum Chemical. Sodium bromide (NaBr) was purchased from Acros Or-

ganics. Hydrochloric acid (HCl, 37%) was purchased from Sigma-Aldrich. Sodium hydroxide (NaOH), N,N-dimethylaminopyridine (DMAP), dichloromethane (CH₂Cl₂), dimethyl-formamide (DMF), dimethyl sulfoxide (DMSO), triethylamine (TEA) were purchased from Fisher. Ethanol (EtOH) and methanol (MeOH) were purchased from Decon Laboratories, Inc. Poly(vinyl alcohol) (PVA) (87.0-89.0% hydrolyzed, MW ~13,000-23,000) was purchased from Thermo Scientific. All materials were used as-received. Reverse osmosis (RO)-purified water was obtained from a centralized source in our campus facility through a tap. A ruby-doped glass sphere (6.35 mm diameter) used for the custom-built probe indenter was acquired from Edmund Optics (NJ, USA) and PTFE spheres (6.35 mm diameter) were obtained from McMaster Carr (IL, USA). Cellulose membrane tubing (1 inch diameter) with a molecular weight cut-off (MWCO) of 3500 was purchased from Sigma Aldrich.

Synthetic Procedures

Synthesis of unmodified polyrotaxane (uPR)

. Adamantane (Ad)-capped unmodified polyrotaxane (uPR) was synthesized from poly(ethylene glycol)dicarboxylate (PEGDC), α -CD, and adamantamine (AdNH₂).

PEGDC. PEG (10g, MW = 35k, 0.3 mmol) was dissolved in RO water (100 mL) maintained at pH 10 with 1 M NaOH solution (100 μ L). TEMPO (100 mg, 0.6 mmol), NaBr (100 mg, 1 mmol), and NaOCl solution (15 mL) were added and the reaction was stirred at room temperature (RT) for 20 min. EtOH/MeOH, equal in amount to NaOCl solution, was added to quench any unreacted NaOCl, followed by dropwise addition of HCl (0.003 M) until the pH was <2, in order to ensure protonation of PEGDC. The polymer was extracted from the aqueous solution into CH₂Cl₂ (3 x 100 mL) and dried under a constant stream of air. The residue was dissolved in hot EtOH (200 mL) followed by overnight refrigeration to precipitate PEGDC, which was collected by vacuum filtration and dried under vacuum at 60 °C to yield PEGDC (6 g, 60%) as a white powder, which was used without further

purification.

Unmodified adamantamide-capped $PEG \subset (\alpha - CD)_n$ polyrotaxane (uPR) was synthesized by a modified literature procedure. ⁶³ PEGDC (3g, 0.09 mmol) was dissolved in RO water (100 mL) and maintained at 80 °C with stirring. α -CD (12g, 12 mmol) was added and the solution was stirred for 30 min until it was no longer turbid. The solution was placed in a refrigerator at 4 °C overnight to precipitate the PEG $\subset (\alpha\text{-CD})_n$ inclusion complex, or pseudo-polyrotaxane (pseudoPR), which was isolated as a white powder by lyophilization (Labconco FreeZone 4.5 L benchtop model) and used without further purification. The crude pseudoPR (~10 g) was dispersed in anhydrous DMF (100 mL). BOP reagent (0.48g, 1.1 mmol), AdNH₂ (1.6g, 1.1 mmol) – obtained from AdNH₂·HCl by washing with aqueous NaOH, extraction in CH_2Cl_2 , and drying by rotary evaporation – and EDIPA (200 μ l, 1.1 mmol) were added to the slurry and the mixture was stirred at RT for 30 min. The slurry was placed in a refrigerator at 4 °C overnight to stopper the pseudoPR, affording the crude unmodified polyrotaxane (uPR). The resulting polymer was purified by centrifugal washing with water, followed by MeOH. The product was dried under vacuum at 70 °C overnight, dissolved in DMSO at a concentration of 10% w/v, and the same precipitation, centrifugation, and drying procedure was repeated a second time to obtain uPR as a white solid $(5.6~\mathrm{g},\,48\%)$. The $^1\mathrm{H}$ NMR spectrum of uPR, consistent with literature, 63 was used to estimate an inclusion ratio of $\sim 27\%$ (corresponding to approximately 106 α -CD rings per chain) by comparative signal integration of the Ad and α -CD resonances (Figure S1(inset)). The molecular weight (MW) of PR was estimated by ¹H NMR spectroscopy to be ~138 kDa, in good agreement with the MW estimation of ~ 130 kDa by gel permeation chromatography (GPC, Figure S2a).

Synthesis of Lipoated Cross-Linkers

Lipoation of α -cyclodextrin (α -CD), and poly(vinyl alcohol) (PVA), and polyrotaxane (uPR) was achieved by esterification of the pendant alcohol moieties of each scaffold (Scheme S1).

Lipoated Polyvinyl Alcohol (LPVA). A roundbottom flask was charged with $\sim 88\%$ hydrolyzed PVA (2g, 130 μ mol, DP ~ 500) and 50 mL anhydrous DMSO and the mixture was stirred under an atmosphere of nitrogen. A solution of LA (10g, 50 mmol) in anhydrous DMSO (25 mL) was added, followed by EDC.HCl (9.6 g, 50 mmol) and TEA (3.6 mL, 28 mmol). The reaction was stirred for 3 days at 35 °C under nitrogen. The product was precipitated in excess MeOH (500 mL), washed over 3 cycles of centrifugation (10 minutes at 3000 rpm) in MeOH, and dried under vacuum at room temperature overnight to obtain LPVA as a brown-colored solid (4 g). The increase in number-averaged MW of ~ 3000 mass units determined by GPC (Figure S2b) corresponds to an average gain of ~ 15 LA units, in good agreement with the $\sim 3\%$ modification ratio determined by NMR signal integration (Figure S3) of selected lipoate and OH signals.

Lipoated Cyclodextrin (LCD). α -CD (2 g, 2 mmol) was dissolved in 50 mL anhydrous DMSO and maintained at 35 °C while stirring under an atmosphere of nitrogen. LA (6g, 28 mmol) was dissolved separately in anhydrous DMSO (50 mL) under the same conditions. The LA solution was added to the α -CD solution, followed by EDC·HCl (5.6g, 28 mmol) and TEA (2 mL, 28 mmol). The reaction was stirred for 3 days at 35 °C under nitrogen. The crude reaction mixture was poured into MeOH (500 mL) and washed over three cycles of centrifugation in MeOH (decanting and replacing the supernatant each time) to obtain a pellet, which was dried under vacuum (overnight) without application of heat to obtain LCD as yellow-tinted white solid (1.2 g). The extent of lipoation was estimated by ¹H NMR spectroscopy (Figure S4) to be ~10 lipoate ester groups per CD ring. The NMR spectrum shows signal broadening indicative of self-assembly, consistent with the known⁶¹

self-assembly of LA $\subset \alpha$ -CD host-guest complexes. Two highly upfield-shifted signals (7.5–8.0 ppm) are consistent with thiol-thiolate hydrogen bonds.⁶⁴ Since these signals are not observed in LPVA and LPR, the stabilization of these hydrogen bonds is likely facilitated by the cavity of the CD host.

Lipoated Polyrotaxane (LPR). uPR (2g, 7μ mol) was dissolved in 50 mL anhydrous DMSO and maintained at 35 °C while stirring under nitrogen. LA (6g, 28 mmol) was dissolved in anhydrous DMSO (50 mL) under the same conditions. Upon complete dissolution of the uPR, the LA solution was added, followed by EDC·HCl (5.6g, 28 mmol) and DMAP (3.6g, 28 mmol). The reaction was stirred for 3 days at 35 °C under nitrogen. An aqueous 1 M NaOH solution (30 mL) was added to the reaction and the contents of the reaction vessel were dialyzed (3500 MWCO cellulose membrane tubing) for 3 days against RO water (4L) to remove unreacted sodium lipoate, replacing the bath with fresh water twice a day. The dialized aqueous solution was lyophilized to obtain a brown solid (2.1 g). The extent of lipoation was estimated by NMR (Figure S1) to be \sim 0.9 lipoate ester groups per CD ring, corresponding to \sim 95 pendant lipoate groups per LPR molecule.

Synthesis of LA-Based Adhesives

The lipoated compounds (LCD, LPVA, or LPR) were mixed with lipoic acid at mass ratios of 0:1, 4:1, 9:1, 99:1, and 1:0 in \sim 2 mL of anhydrous DMSO at a concentration of 20 % w/v. After stirring the solutions overnight at \sim 80 °C, 100 μ L of the homogeneous solution was cast into a circular silicone mold (8 mm diameter x 500 μ m thickness) on top of polyimide tape (Kapton, used to transfer samples onto the adhesive testing setup) affixed to a glass microscope slide, avoiding air bubbles at the interface, and placed in an oven maintained at 80 °C for approximately 4 h. This cast-and-dry procedure procedure (see Figure 1) was repeated twice to increase the thickness of the resulting adhesive films. After the final casting step, the samples were left in an oven at 80 °C for \sim 12 hours to evaporate DMSO completely

and initiate the ring-opening polymerization of LA, which only occurs above its melting point of ~ 70 °C. ²⁴ Sample thicknesses, determined by the dynamic mechanical analyzer while preindenting the sample until a non-zero force is observed, varied between 500–800 μ m. The pre-adhesive solutions were also cast directly on glass to capture photographs (see Figure 1) of the adhesives without the yellow background color of Kapton, and for the load-bearing tests.

Characterization Procedures

NMR Spectroscopy

Nuclear Magnetic Resonance (NMR) spectroscopy was performed on a Bruker Avance-III 300 MHz NMR spectrometer at room temperature and spectra were analyzed in MestReNova software (v14). The spectra were referenced to the residual solvent signal (2.50 ppm for $(CD_3)_2SO$).

Gel Permeation Chromatography.

Gel permeation chromatography (GPC) was performed on a Tosoh EcoSEC 8320 system equipped with columns for DMSO as the solvent. MW estimates were determined using PEG standards of known MW as calibrants in DMSO.

Probe-Tack Tests

The work of debonding for all of the adhesive formulations were measured using a dynamic mechanical analyzer (Anton Paar MCR-702) with a custom-built compression plate that serves as a probe indenter. The indenter fabrication and testing was similar to protocols reported in the literature. The probe was constructed by bonding either a glass or PTFE (6.35-mm diameter) sphere securely on a flathead screw with high weld strength epoxy glue (J-B ClearWeld) and allowed to cure for at least 1 hour. Upon ensuring sufficient adhesion between the sphere and screw, the screw side of the assembly was affixed to an

8-mm rheometer parallel plate (Anton Paar) with the epoxy glue. The red color of the ruby-doped glass sphere was leveraged to enhance contrast with the background in the photographs for accurate determination of contact area.

Thermal Behavior

Melting point and glass transition of the adhesives were measured using differential scanning calorimetery (DSC). DSC Q2000 (TA Instruments) with a constant supply of nitrogen was used to perform a heating run on the samples to determine the glass transition temperature (T_g) and melting behavior. A ramp rate of 10 °C was used to heat the sample from -80 °C to 100 °C. Degradation profile of the adhesives was determined by thermogravimteric analysis (TGA). TGA 5500 (TA instruments) was used to heat the samples from room temperature to 600 °C to elucidate the degradation behavior. The degradation profiles confirmed that the samples were cast at a temperature where the adhesives are thermally stable. The highest temperature used for DSC studies is also within the stable temperature window.

X-ray Scattering

The crystallinity of the adhesive specimens was characterized using Forvis Technologies wideangle X-ray scattering (WAXS) 30 W Xenocs Genix3D X-ray source (Cu anode, wavelength λ = 1.54 Å) and Dectris Eiger R 1 M detector. The data were collected at a sample-to-detector distance of 145.66 mm, while the samples were exposed to X-rays for 3 minutes.

Rheology

The rate-dependent properties of the adhesive formulations were characterized by shear rheology on an Anton-Paar MCR-702 rheometer. Amplitude sweeps in the strain range of 0.001–0.1% were carried out for all adhesive samples to ascertain the linear viscoelastic (LVE) limit. The exception to this strain range was the commercial adhesive (UHU Tac) used for comparison, which required a lower strain range of 0.0001–0.01% to determine the

LVE. A strain (varying between 0.01 - 0.05%) well within the respective LVE limits of the samples was chosen to perform frequency sweeps. The storage (G') and loss (G'') moduli were recorded as a function of frequency between 0.1–100 rad/s. An 8-mm parallel plate was used to deform and record mechanical spectra while a 25-mm plate served as the bottom plate. To align with the conditions for probe-tack tests, all rheological experiments were carried out at room temperature $(22 \pm 1 \, {}^{\circ}\text{C})$.

Load-Bearing Tests

The load-bearing capacity of the top-performing adhesive formulation we tested (LA/LPR 99:1) was demonstrated by suspending a 100 g weight from two glass or PTFE slides bonded together by the adhesive. A solution of 99:1 LA:LPR in DMSO (20 %w/v) was poured into the same silicone molds (8mm diameter x 500μ m thick), illustrated in Figure 1. Diffusion of DMSO into the silicone mold was deemed minimal since no swelling, hazing, discoloration, cracking or wrinkling was observed in the mold. In this case, the molds were placed directly on a glass microscope slide or a PTFE strip cut to approximately the same size as the glass slide. The same multi-step solution casting procedure described earlier and illustrated in Figure 1 was used to deposit the adhesive on the plates. The two slides – one coated, one uncoated – were bonded together under light pressure applied by hand, then placed under a 1-kg weight to ensure that pressure was applied uniformly and reproducibly. A 100g standard weight was suspended from the adhered slides by a metal wire (hung from a paper clip bonded to one glass slide with epoxy) in air or in a 4L Erlenmeyer flask filled with water. A similar load-bearing test was employed for the 99:1 LA:LPR sample with a 4 kg weight comprising a glass bottle containing water. A video demonstration of the load bearing capacity is available in the supplementary information.

Results and discussion

The aim of this work is to lay a foundation for developing advanced pressure-sensitive adhesives (PSAs) based on poly(lipoic acid) using only bio-friendly materials. In our approach, we prepared several lipoated additives derived from biocompatible scaffolds – α -CD, PVA, and PR – to be employed as cross-linkers in the ring-opening polymerization of LA.

Synthesis of Lipoated Cross-Linkers Cross-linkers are employed in poly(LA) adhesives to increase MW and prevent depolymerization. ²² In order to synthesize poly(LA) adhesives with bio-friendly cross-linkers, we functionalized the α -CD, PVA, and PR scaffolds *via* esterification ^{67,68} of their hydroxyl groups with lipoic acid and EDC·HCl (Scheme S1). The successful lipoation of each compound was confirmed by ¹H NMR spectroscopy (Figure S1, S3, S4) and GPC (Figure S2). Lipoated PVA (LPVA) was isolated with an average of \sim 15 lipoic ester groups per macromolecule. LPVA was prepared as a fixed-crosslink control for comparison with the host-guest cross-linker comprising lipoated α -CD (LCD), which was isolated with an average of \sim 10 LA groups per molecule, as well as a sliding-crosslink scaffold based on lipoated polyrotaxane (LPR), which was obtained with an average of \sim 0.9 CD rings per chain, corresponding to \sim 95 lipoate groups per macromolecule.

Library of LA-Based Adhesive Formulations We leverage the thermally activated self-polymerization of LA²⁴ in the presence of lipoated cross-linkers to prepare adhesive viscoelastic polymers. Varying mass ratios of LA and cross-linker (either chemical³⁰ or physical²²) leads to changes in adhesive behavior. To help uncover patterns in structure-property relationships, we varied network structure by preparing mixtures of LA with each cross-linker at mass ratios of 0:1, 4:1, 9:1, 99:1, and 1:0 in concentrated DMSO solutions (20% w/v). These solutions were cast in a circular silicone mold on Kapton tape or glass and oven-dried at 80 °C (above the melting point of LA) to obtain the adhesives (Figure 1). Thermogravimetric analysis of the adhesives shows no mass loss from the samples below 150

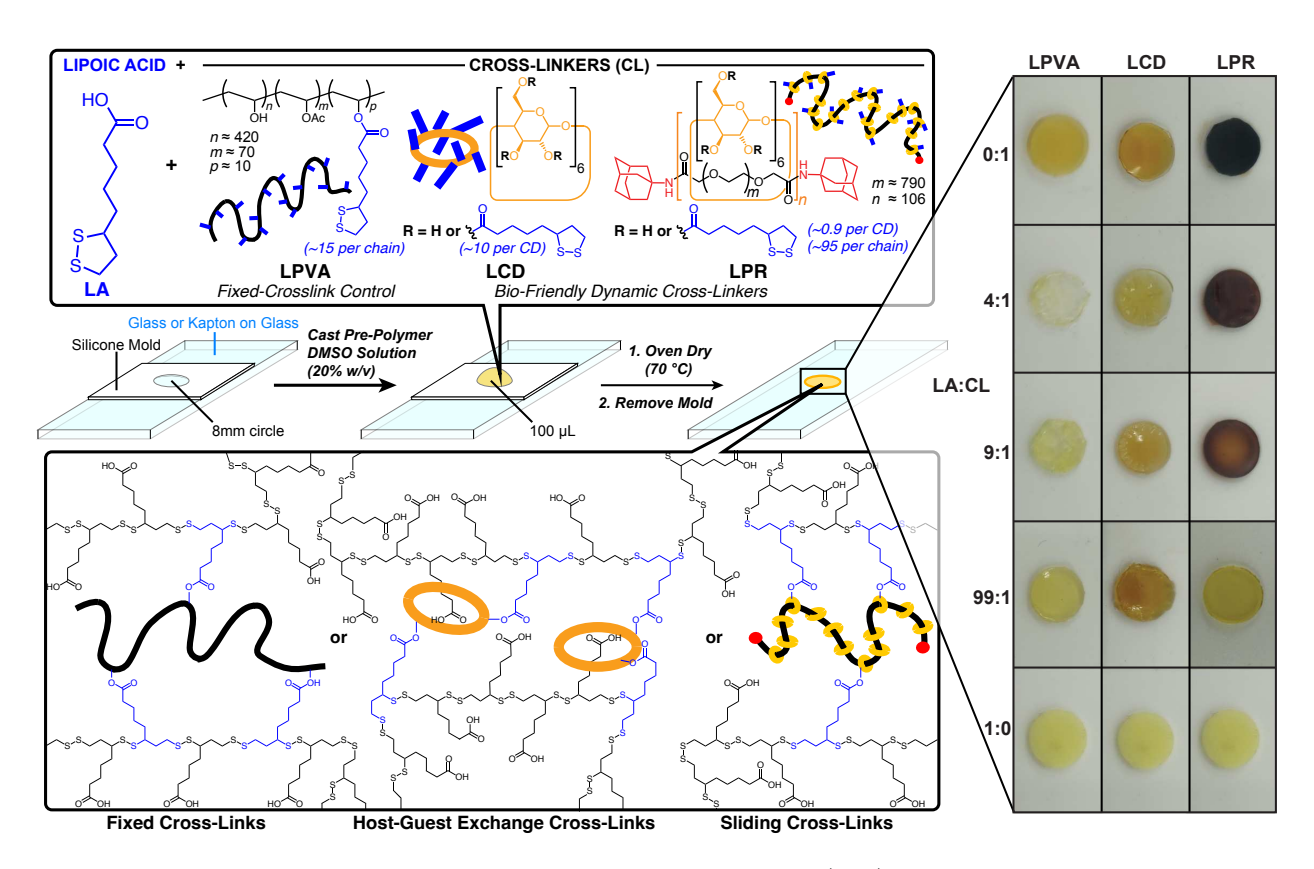


Figure 1: Graphical schematic of the process by which poly(LA) adhesives are produced upon ring-opening polymerization of LA in the presence of LPVA, LCD, or LPR cross-linkers, and photographs of the adhesive formulations as-cast.

°C (Figure S5), unlike a pure DMSO sample which loses all mass by 150 °C. Since each cross-linker is decorated with multiple pendent lipoic esters, we expect their dithiolane moieties to become randomly incorporated²³ in the poly(LA) chains as they grow and exchange bonds during thermal self-polymerization, resulting in a branched macromolecular network (Figure 1). Photographs of each adhesive polymer on glass are shown in Figure 1. The 1:0 sample of pure poly(LA) crystallizes rapidly and appears opaque, unlike the cross-linked mixtures which are more transparent, indicating lower crystallinity. We observed that the cross-linked mixtures also become more opaque over time (1–3 weeks), except for those based on LPR, which retain their translucent appearance for at least 4 months.

Probe-Tack Tests on Glass and PTFE We employed 6.35-mm spherical probes of glass or PTFE to evaluate the adhesion of our formulations on a dynamic mechanical analyzer,

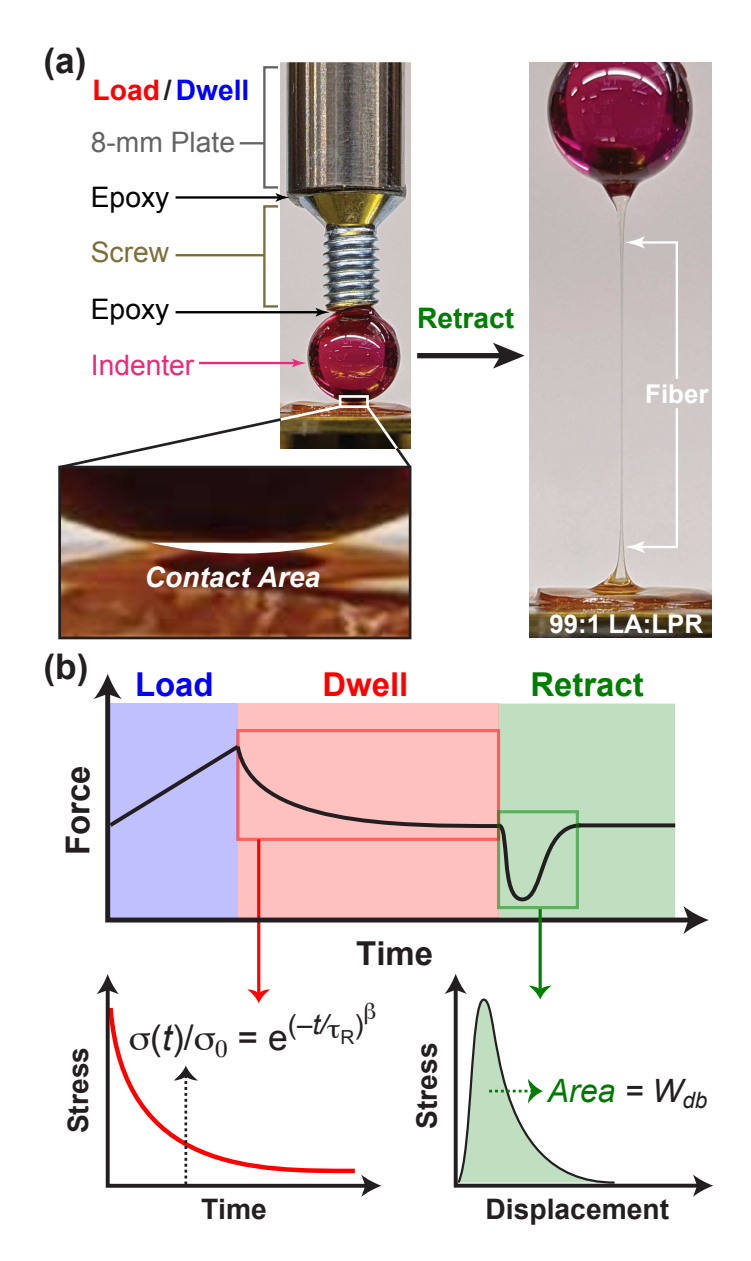


Figure 2: Overview of probe-tack testing setup and analysis. (a) Photographs of the spherical probe (with parts labeled) in the dwell and retraction phases of a probe-tack test on 99:1 LA:LPR. (b) Conceptual schematic showing how the force vs. time data is processed to determine the relaxation time (τ_R) using the KWW function and work of debonding (W_{db}) by integrating the area under the stress vs. displacement curve.

inspired by recent reports employing spherical probes. 65,66,69 The probe-tack tests are divided into three stages (Figure 2): load, dwell, and retract. First, the probe is brought into contact with the surface while being lowered slowly until a non-zero force (~ 0.01 N) is registered. The sample is then indented to a depth of 20 μ m over 0.5s ("loading"). Then, in the

dwelling stage, the loaded sample is allowed to relax for 120 s while measuring data on the attenuation of force. The 120-s time interval, chosen to maintain consistency across all samples, was long enough for most samples to reach their σ_0/e values. Finally, the probe is immediately retracted at a rate of 0.1 mm/s until adhesive failure or a displacement of 50mm (whichever occurs first) at a rate of 0.1 mm/s. Representative photographs of indentation and retraction of 99:1 LA:LPR are shown in Figure 2a. Force is measured as a function of time throughout the test. The work of debonding (W_{db}) is calculated from the retraction data and the relaxation time (τ_R) is calculated from the dwell data.

Work of Debonding We measure the work of debonding (W_{db}) as an indicator of adhesive energy. The W_{db} values are calculated by integration of the stress vs. displacement graphs generated during retraction of the probe. Representative examples of the stress vs. displacement graphs obtained from all adhesive formulations are shown in Figure S6 for the glass probe and Figure S7 for the PTFE probe. Each probe-tack test was repeated in triplicate and the average W_{db} values were compared on glass (Figure 3a) and PTFE (Figure 3b). Several clear trends are observed with respect to the effect of LA:cross-linker ratio and substrate material.

Effect of LA:Cross-Linker Ratio on Glass. In general, the work of debonding increases substantially with increasing LA content, but pure LA is a poor adhesive ($W_{db} \approx 10$) owing to its crystallinity. The 99:1 LA:cross-linker mixtures exhibit the highest W_{db} values in all cases. On glass, all three 99:1 formulas show very strong adhesion, with W_{db} values exceeding 1000 J/m², higher than the commercial PSA (UHU Tac, $W_{db} \approx 900$ J/m²). Among all of the PSAs we tested, the 99:1 LA:LCD formula forms the strongest bond with an average work of debonding of 2500 J/m². However, the LA:LPR mixtures are the least sensitive to the cross-linker ratio, with the 4:1 and 9:1 formulas each matching UHU Tac, which is 5–6-fold stronger than the corresponding 4:1 and 9:1 LCD and LPVA adhesives. The 4:1 and 9:1 LA:LCD formulas, hardened by crystallinity, showed poor adhesion. The cause of

this relatively high crystallinity (especially in 9:1 LA:LCD, Figure S10b), remains an open question.

Effect of the Substrate Material. PTFE is an inert, hydrophobic polymer with low surface energy commonly used as a non-stick coating. Whereas polylipoates can hydrogen bond with surface-bound oxygen atoms on glass, the supramolecular bridging interactions between carboxylates and fluoropolymers are weaker. 2,22,70 Thus, as expected, 70,71 W_{db} is lower on PTFE for all formulations. Unlike the case of glass, the bio-friendly 99:1 mixtures based on the supramolecular LCD and LPR scaffolds outperform 99:1 LA:LPVA by an order of magnitude on PTFE, each with remarkably strong bonds ($W_{db} \approx 400$), also fourfold stronger than UHU Tac. On PTFE, where surface adhesion is less significant, the differences between the CD-based cross-links and the PVA-based cross-links are amplified. PTFE reduces the work of debonding by a factor of \sim 4 in 99:1 LA:LCD and LA:LPR, compared to a factor of 37 for LA:LPVA. The presence of mobile cyclodextrins are the key difference between these cross-linkers, likely improving the material's resistance to deformation by way of dynamic binding site exchange or ring sliding motions (i.e., the pulley effect 53,59,60), respectively.

Effect of Stress Relaxation Stress relaxation data can provide insight into an adhesive's internal processes on the molecular scale. For example, the self-diffusivity of polymers is inversely proportional to the relaxation time $\tau_{\rm R}$.⁷² Larger self-diffusivity values contribute to high molecular mobility which endows an adhesive with the ability to comply and exhibit good tensile strain.⁵⁵ The ability of a soft material to relax fast allows it to "switch" easily between the elastic state and viscous state. PSAs should be able to dissipate any deformation in the adhered state but also retain micro- and macrostructure during debonding, ⁷³ which is why they are viscoelastic in nature and possess fast relaxation times. Fast relaxation times ensure that the PSA can deform quickly enough to form a good interfacial contact with the substrate, and also minimize the transfer of adhesive material to the bonded substrate.

We estimated relaxation times (τ_R) in our adhesives by fitting (Figure S8) the dwell curves

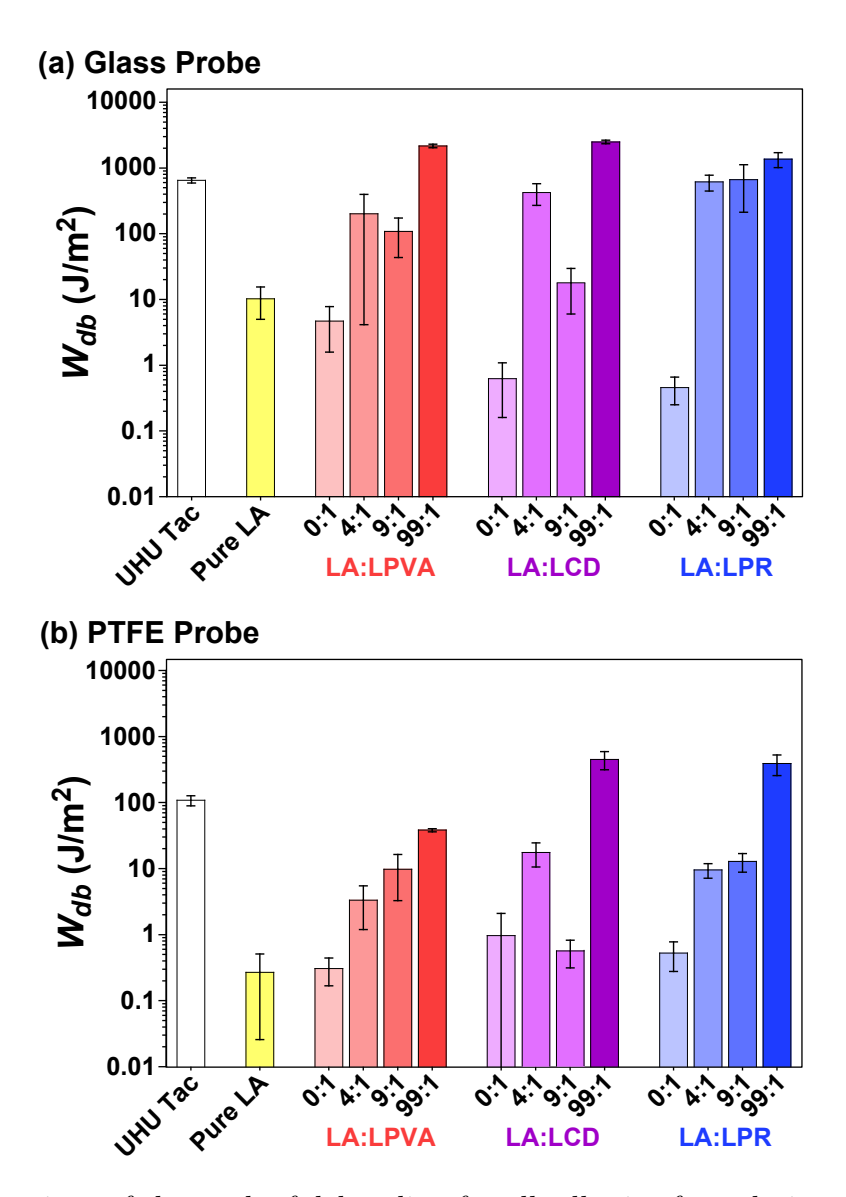


Figure 3: Comparison of the work of debonding for all adhesive formulations with probes of (a) glass and (b) PTFE. The dwell time was 120 s and the retraction rate was 0.1 mm/s for all samples.

to the empirical stretched exponential Kohlrausch–Williams–Watts 74 (KWW) function:

$$\frac{\sigma(t)}{\sigma(0)} = e^{(-t/\tau_R)^{\beta}} \tag{1}$$

where t is time and and β is a stretching factor used to indicate the broadness of the relaxation process associated with τ_R . The Maxwell stress relaxation function $(\sigma(t)/\sigma(0) = e^{(-t/\tau_R)})$ did not produce a good fit (R² < 0.6) implying that the relaxation observed in the LA-based

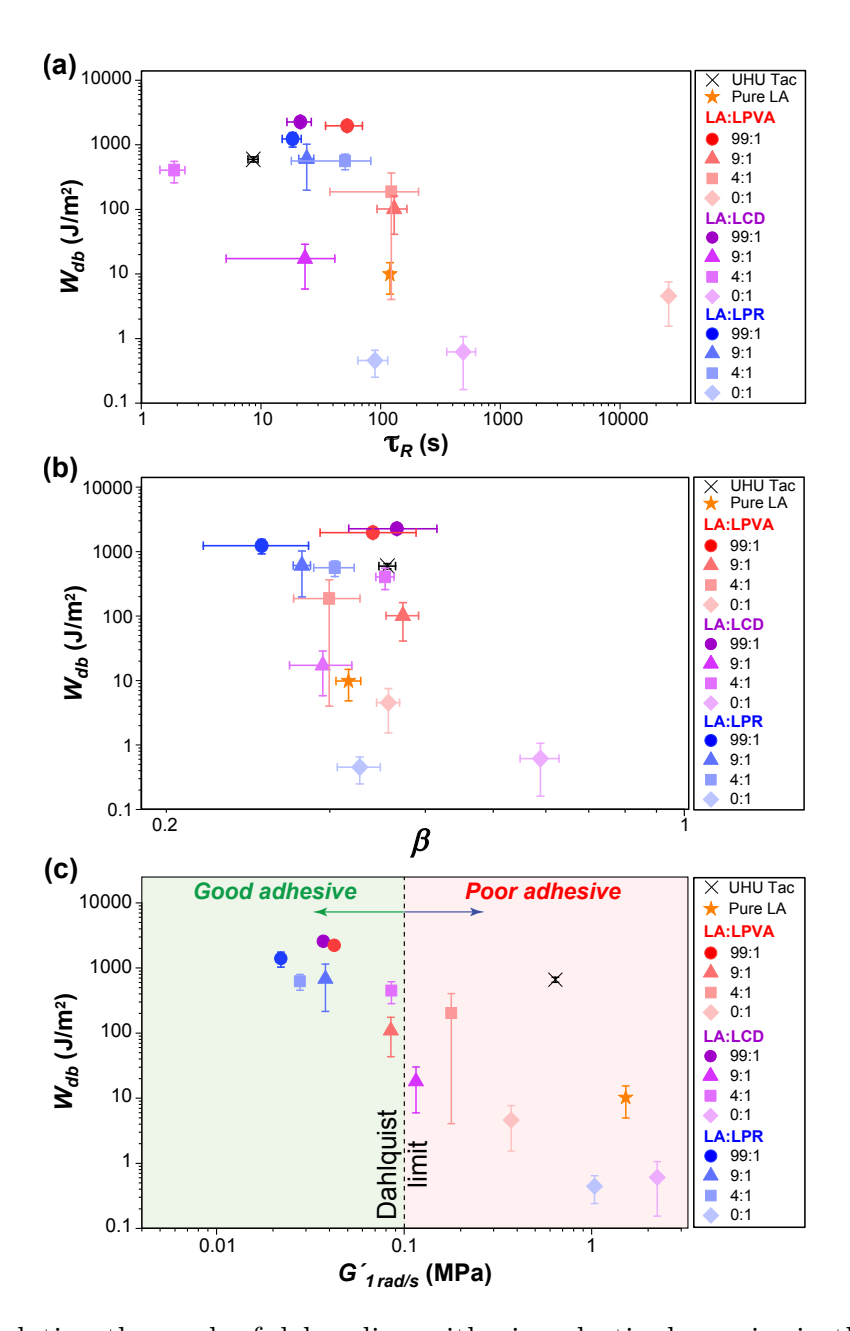


Figure 4: Correlating the work of debonding with viscoelastic dynamics in the polymer adhesives. (a) A plot of W_{db} vs $\tau_{\rm R}$ shows an inverse correlation between adhesion strength and relaxation time. (b) A plot of $W_{\rm db}$ vs β shows that the stronger adhesives with increasing LA content tend to have lower β values, indicating that inhomogeneities increase with increasing LA content. (c) A plot of W_{db} vs G' shows an inverse correlation between adhesive bond strength and storage modulus at a frequency of 1 rad/s, in agreement with the Dahlquist criterion for adhesives (visualized by a dashed line and red/green shading).

adhesives is not governed by a single relaxation process, but could arise instead from multiple coupled processes. The KWW equation has been widely used to model nonlinear processes in

polymeric and soft material systems. ^{77–79} The KWW function applied to latex adhesives has revealed the effect of atmospheric conditions, additive concentration, and substrate effects on the cooperativity of their relaxation processes. ⁸⁰ Small-scale localized motions can also be distinguished from larger segmental motions using KWW relaxation. ⁸¹ In a recent study, ⁸² $\tau_{\rm R}$ increased and β values decreased as more cross-links were introduced. The reduction in β values indicates a diminishing cooperativity between polymer segments, associated with retardation of segmental relaxation due to cross-linking.

The effect of stress relaxation in PSAs is not yet completely understood; $\tau_{\rm R}$ and adhesion energy are well correlated in some PSAs,^{83,84} but uncorrelated in others.^{85,86} In the case of our LA-based adhesives, the work of debonding tends to increase with decreasing relaxation times (Figure 4a). With the exception of 99:1 LA:LPVA, the high-LA-content adhesives exhibit short relaxation times ($\tau_{\rm R}$ <30 s), as does the commercial adhesive sample (UHU Tac, $\tau_{\rm R}$ = 8.5s). The shorter relaxation time manifests as a "snap-off" (a term used to describe adhesive or cohesive failure)⁸⁷ when an adhesive is retracted at a faster rate, which agrees with trends reported in the literature.⁶⁵ Likewise, the poor adhesives with low LA content exhibit much longer relaxation times, interfering with their ability to rapidly dissipate energy.

The cooperativity of the adhesives (as indicated by the magnitude of β) appears inconsistent within each adhesive series, but in general the β values decrease as lipoic acid content increases (Figure 4b). The reduction in β values suggests an increase in dynamic and/or structural inhomogeneity, which may also enhance adhesion.⁸⁸ Inhomogeneities in our samples could arise from the dangling poly(lipoic acid) chains, due to the incomplete gelation of LA, or poly(lipoic acid) cyclic polymers which form in the case of racemic mixtures of LA.²⁴ Thus, the stress relaxation data obtained from the probe-tack tests indicates that the strongest adhesives generally have shorter relaxation and more network inhomogenities.

Rate-Dependent Investigations of the Adhesives Since the dynamic mechanical properties of viscoelastic polymers are frequency dependent, it follows that their adhesion properties are likewise rate dependent. We investigated the rate dependence of our adhesive formulas by shear rheology and probe-tack tests of increasing retraction rate.

Shear Rheology The correlation between viscoelastic moduli and adhesion has been established ^{89,90} since the pioneering work of Dahlquist ⁹¹ in the 1960s. We employed shear rheology (Figure S9) to further investigate correlations between the mechanical properties of the poly(LA) formulas and their adhesion on glass. Frequency sweeps carried out at room temperature (22±1 °C) over a frequency range of 0.1–100 rad/s reveal how sensitive the LA:LPVA (Figure S9a), LA:LCD (Figure S9b), and LA:LPR (Figure S9c) mixtures are to perturbation rates, and show that all of the networks soften with increasing LA content. The strain was below the linear viscoelastic limit in all frequency sweeps, as determined by amplitude sweeps in the range of 0.001–0.1 %.

 W_{db} is plotted against the storage modulus at 1 rad/s ($G'_{1 rad/s}$) in Figure 4c in order to reveal the inverse correlation between W_{db} and $G'_{1 rad/s}$, expected and explained by the Dahlquist criterion, ⁹¹ which suggests that superb adhesives are soft with moduli ≤ 0.1 MPa. The dynamic mechanical properties of the inspirational poly(LA) adhesives treated with divinyl and iron cross-linkers also meet the Dahlquist criterion for soft adhesives. ²²

Effect of Retraction Rate To investigate the rate dependence of adhesion, we performed probe-tack tests at increasing retraction rates ($V_{\rm ret}$) of 0.1, 1, and 10 mm/s (Figure 5a–d). On glass, photographs (Figure 5a) show the formation a filament during retraction, which remains unbroken as the sample is stretched up to 50 mm at retraction rates of 0.1 or 1 mm/s, whereas the filament snaps off at a displacement of 6.8 mm at 10 mm/s. On PTFE (Figure 5b), adhesive failure occurs at a shorter distance (0.88 mm at $V_{\rm ret} = 0.1$ mm/s, 0.58mm at $V_{\rm ret} = 1$ mm/s, 0.66 mm at $V_{\rm ret} = 10$ mm/s). In general, a trend of increasing W_{db} is observed with increasing $V_{\rm ret}$. This effect is most pronounced for 99:1 LA:LCD on

glass (Figure 5c), which is remarkably strong ($W_{db} = 23,000 \text{ J/m}^2$ at 1 mm/s and 18,000 J/m² at 10 mm/s). The 99:1 LA:LPR bond is also very strong ($W_{db} = 13,000 \text{ J/m}^2$) at 10 mm/s.

The increase in work of debonding can be related to the frequency sweep data in Figure S9, since V_{ret} can be equated ⁹² to the rheological angular frequency (ω) by the equation 2:

$$V_{ret} = \frac{h\omega}{2\pi} \tag{2}$$

where h is the sample thickness. Using this relation we attempt to correlate the adhesive behavior of a sample with features of its rheological frequency sweep. Considering the 99:1 LA:LPR sample, we observe that the ω is 1.2 rad/s at $V_{\rm ret}=0.1$ mm/s (with the value of h being 0.520 mm, based on the sample thickness used for rheology). We do not observe a significant change in work of debonding for 99:1 LA:LPR composites between $V_{\rm ret}$ of 0.1 and 1 mm/s but as we proceed to 10 mm/s the adhesion energy increases significantly. This rate-dependent adhesive behavior can be tracked to the dynamic moduli at the corresponding ω values. At \sim 1.2 rad/s and \sim 12 rad/s the storage and loss modulus are significantly far apart but at higher frequencies, the viscous dissipation increases considerably making the formulation a stronger adhesive. An elastic material with good viscous dissipation exhibits excellent adhesion properties. Similarly, the rate dependence of the other adhesives can be correlated to their frequency sweep data. The rheological frequency sweep of 0.1–100 rad/s covers all associated $V_{\rm ret}$ values for the samples tested at different retraction rates.

Effect of Aging. Without cross-links, poly(LA) crystallizes within minutes below its melting temperature as a result of nucleating oligomers that drive ring-closing depolymerization of longer polymer chains with terminal radicals. ^{22,30} XRD (Figure S10) and DSC (Figure S11) data reveal that this crystallization process is retarded substantially in all of the cross-linked formulations, since the signals associated with LA diffraction and melting, respectively, are highly attenuated in the adhesives. Since we do not employ vinylic monomers to capture

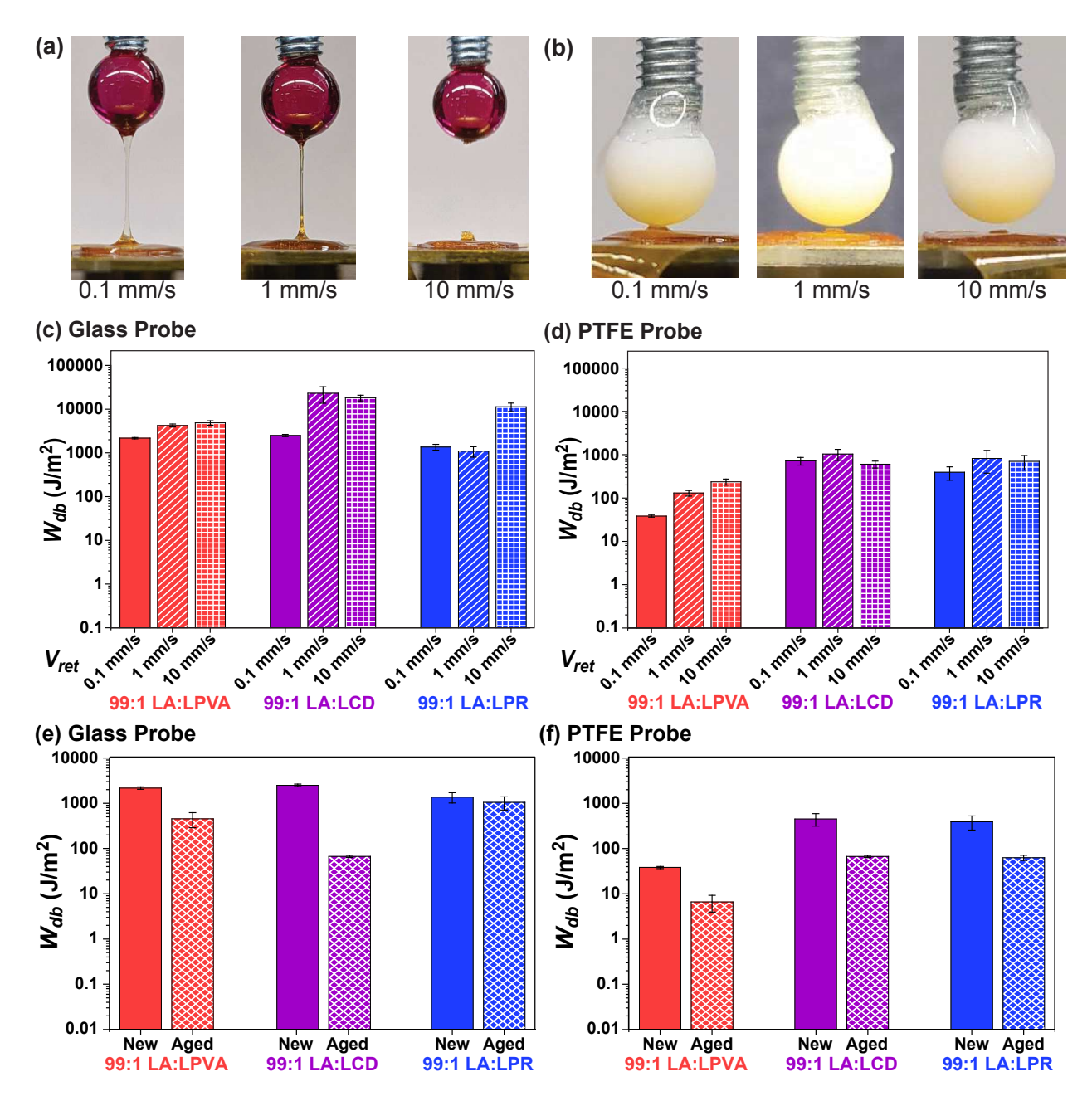


Figure 5: Effects of retraction rate and aging on top-performing 99:1 LA:cross-linker adhesives. Photographs show the filament snap-off occuring sooner at faster retraction rates in both (a) glass and (b) PTFE probes, while the work of debonding generally increases with retraction rate on (c) glass and (d) PTFE. The effect of aging (four weeks in open air) on the work of debonding is also summarized for (e) glass and (f) PTFE.

these radicals and stabilize the polydisulfide chains, we felt it necessary to determine if aging could diminish adhesive performance by way of crystallization. The work of debonding in fresh samples (aged a few hours after removing from the oven) and aged samples (incubated

in ambient air for 4 weeks) is compared for each of the the 99:1 LA:cross-linker formulas on glass and PTFE in Figure 5e-f. All samples retained their shape and form (no observed flow) over the 4-week aging period. All of the aged samples exhibit diminished W_{db} values, the extent of which varies considerably. On glass (Figure 5e), the aged 99:1 LA:LPR sample does not suffer a statistically significant loss in adhesion energy, whereas W_{db} drops down to $450~\mathrm{and}~70~\mathrm{J/m^2}$ in the aged 99:1 formulas of LPVA and LCD, respectively. By contrast, on PTFE the W_{db} values observed for PSAs based on LCD and LPR are almost identical, each falling to $\sim 70 \text{ J/m}^2$ upon aging. The less adhesive 99:1 LA:LPVA sample is diminished to a similar extent, from ~ 400 to ~ 70 J/m², upon aging. Comparisons of XRD data (Figure S12) in fresh and aged samples revealed that crystalline domains of LA emerge gradually in the cross-linked samples, but with the 99:1 LA:LPR formula showing only minimal crystallinity even after 4 weeks. In accordance with literature data, 94 the peaks that appear over time at 2θ values of 17, 18.5, 21 and 22 are attributable to these crystalline domains of lipoic acid. In agreement with the XRD data, the DSC data (Figure S13) reveals stronger signals associated with the heat of fusion of LA in the aged samples. We conclude that all of the adhesive formulas undergo molecular rearrangements that degrade adhesive performance, likely owing to the slow formation of micro-crystalline domains, but this undesirable effect is highly suppressed by the polyrotaxane cross-linker, at least when bonding to glass.

Load-Bearing Demonstrations in Air and Water We selected the 99:1 LA:LPR adhesive for further demonstrations of load-bearing performance, since it was found to be the most resistant to age-related loss of tack. 40 mg of the adhesive was prepared on glass or PTFE slides, which were bonded together with uncoated slides in a sandwich geometry under the external pressure of a 1-kg weight for at least 2 hours, in an oven at 60 °C, to ensure consistent thermal and pressure treatment. A 100-g weight was then affixed from the sandwich assembly and suspended from it under the force of gravity. The adhesive bears the weight without failure for 24 hours on both substrates (Figure 6a). In the absence of a base



Figure 6: Demonstration of load-bearing ability of the 99:1 LA:LPR adhesive using PTFE and glass. (a) The glass (top) and PTFE (bottom) adhered assembly with 40 mg adhesive was able to bear a 100 g weight in air and water. (b) A 4 kg weight was suspended with 100 mg of adhesive on glass.

or salts, poly(LA) is hydrophobic.²⁹ Recent work⁹⁵ has predicted that water is structured around LA-modified polyrotaxane out to a distance of 5 Å from its surface, beyond which water is considered unstructured and free. These considerations led us to reason that the 99:1 LA:LPR adhesive might also perform well underwater, with the structured water layer providing a screen to prevent aqueous swelling. Indeed, the 40 mg of adhesive also bears the 100-g weight under water for 24 hours. A significantly higher load of 4 kg was lifted using 100 mg of the 99:1 LA:LPR adhesive formulation on glass (Figure 6b). These initial load-bearing tests validate the excellent performance of the age-tolerant 99:1 LA:LPR adhesive formula.

Conclusion

Strong pressure-sensitive supramolecular adhesives can be formulated from poly(lipoic acid) and lipoated cross-linkers present at only 1% w/v concentration (compared with 20% in prior work²²). Importantly these PSAs can be all-organic and bio-friendly, and devoid of

any metal ions or petroleum-based cross linkers (in the case of lipoated cyclodextrin). The petroleum-based PEG backbone of the polyrotaxane cross-linker can be replaced in principle by green polymers such as poly(lactic acid), 96 poly(ε -lysine), 97 or silk fibroin, 98 although we cannot predict how it would impact material properties. The bio-friendly supramolecular PSAs exhibit high energies of debonding from both glass and poly(tetrafluoroethylene) that exceed the petroleum-based controls. The 99:1 LA:cross-linker formulas exhibit strong adhesion (up to 2500 J/m^2 on glass and 450 J/m^2 on PTFE at a 0.1 mm/s retraction rate), outperforming a commercial PSA. The work of debonding (W_{db}) tends to increase with decreasing cross-linker ratio, as well as increasing retraction rate $(V_{\rm ret})$ up to 10 mm/s. We also observed that W_{db} generally correlates inversely with the stress relaxation times (τ_R) and the viscoelastic moduli (G', G'') measured by indentation tests and shear rheology, respectively. Unlike in pure poly(lipoic acid), a poor adhesive which rapidly crystallizes via ring-closing depolymerization, ^{22,30} the lipoated cross-linkers retard crystallization substantially, but not completely. While the strongest adhesive was found to comprise a 99:1 ratio of LA:LCD when freshly prepared ($W_{\rm db} > 20{,}000~{\rm J/m^2}$ at $V_{\rm ret} = 10~{\rm mm/s}$), only the 99:1 LA:LPR formula on glass, which forms only a slightly weaker bond than 99:1 LA:LCD, is resistant to significant loss in tack upon aging for 4 weeks. Understanding mechanistically how LPR suppresses aging in poly(LA) would require further research converging models and time-resolved data.

The bio-friendly supramolecular cross-linkers also outperform the non-supramolecular petroleum-based LPVA polymer employed as a control, especially on PTFE. We thus infer that their supramolecular dynamics – host-guest exchange in the case of LCD, ring-sliding in the case of LPR – enhances adhesion, likely by providing pathways to dissipate mechanical stress as the adhesive is deformed, and by retarding crystallization. The strong and temporally stable slide-ring adhesive (99:1 LA:LPR) was further subjected to load-bearing tests, with 100 mg of aged material easily withstanding the force of a suspended 4-kg weight in air and a 100-g weight underwater. More comprehensive structure-property investigations into

the effects of inclusion ratio (number of threaded CD rings per PR chain), extent of lipoation, and other substrate compositions will be the subject of future work, as well as their stimulus-responsive, recyclable, and self-healing properties. These supramolecular adhesives may be of particular interest for applications in biomedicine or sustainable materials that demand eco- and bio-friendly macromolecules.

Acknowledgement

This work was supported by funding from the College of Engineering and Applied Science at the University of Colorado Boulder and the National Science Foundation (Award No. 2023179). The authors gratefully acknowledge use of the Materials Research X-Ray Diffraction Facility at the University of Colorado Boulder (RRID: SCR019304), with instrumentation supported by NSF MRSEC Grant DMR-1420736.

Supporting Information Available

The Supporting Information is available free of charge at

¹H NMR spectra of lipoated crosslinkers, GPC data, TGA data for all formulations, stress vs. displacement plots for all formulations on glass and PTFE, KWW fits of stress relaxation data, rheological frequency sweeps, XRD spectra for all formulations, DSC data for all formulations.

References

(1) Stupp, S. I.; LeBonheur, V.; Walker, K.; Li, L.-S.; Huggins, K. E.; Keser, M.; Amstutz, A. Supramolecular Materials: Self-organized Nanostructures. *Science* **1997**, *276*, 384–389.

- (2) Shi, C.-Y.; Zhang, Q.; Tian, H.; Qu, D.-H. Supramolecular Adhesive Materials from Small-Molecule Self-Assembly. *SmartMat* **2020**, *1*, e1012.
- (3) Chen, S.; Li, Z.; Wu, Y.; Mahmood, N.; Lortie, F.; Bernard, J.; Binder, W. H.; Zhu, J. Hydrogen-Bonded Supramolecular Polymer Adhesives: Straightforward Synthesis and Strong Substrate Interaction. *Angewandte Chemie* **2022**, *134*, e202203876.
- (4) Ren, J.; Li, M.; Wang, X.; Li, Y.; Yang, W. Adhesive hydrogels with toughness, stretch-ability, and conductivity performances for motion monitoring. *Polymer Bulletin* **2022**, 1–17.
- (5) Cui, C.; Gu, R.; Wu, T.; Yuan, Z.; Fan, C.; Yao, Y.; Xu, Z.; Liu, B.; Huang, J.; Liu, W. Zwitterion-Initiated Spontaneously Polymerized Super Adhesive Showing Real-Time Deployable and Long-Term High-Strength Adhesion against Various Harsh Environments. Advanced Functional Materials 2022, 32, 2109144.
- (6) Das, S.; Rodriguez, N. R. M.; Wei, W.; Waite, J. H.; Israelachvili, J. N. Peptide Length and DOPA determine Iron-Mediated Cohesion of Mussel Foot Proteins. *Advanced Func*tional Materials 2015, 25, 5840–5847.
- (7) Gebbie, M. A.; Wei, W.; Schrader, A. M.; Cristiani, T. R.; Dobbs, H. A.; Idso, M.; Chmelka, B. F.; Waite, J. H.; Israelachvili, J. N. Tuning Underwater Adhesion With Cation-π Interactions. *Nature Chemistry* 2017, 9, 473–479.
- (8) Xu, Y.; Ji, Y.; Ma, J. Hydrophobic and Hydrophilic Effects in a Mussel-Inspired Citrate-Based Adhesive. *Langmuir* **2020**, *37*, 311–321.
- (9) Holten-Andersen, N.; Jaishankar, A.; Harrington, M. J.; Fullenkamp, D. E.; Di-Marco, G.; He, L.; McKinley, G. H.; Messersmith, P. B.; Lee, K. Y. C. Metal-Coordination: Using One of Nature's Tricks to Control Soft Material Mechanics. *Journal of Materials Chemistry B* 2014, 2, 2467–2472.

- (10) Li, Y.; Qin, M.; Li, Y.; Cao, Y.; Wang, W. Single Molecule Evidence for the Adaptive Binding of DOPA to Different Wet Surfaces. *Langmuir* **2014**, *30*, 4358–4366.
- (11) Heinzmann, C.; Coulibaly, S.; Roulin, A.; Fiore, G. L.; Weder, C. Light-Induced Bonding and Debonding With Supramolecular Adhesives. ACS Applied Materials & Interfaces 2014, 6, 4713–4719.
- (12) Du, R.; Wu, J.; Chen, L.; Huang, H.; Zhang, X.; Zhang, J. Hierarchical Hydrogen Bonds Directed Multi-Functional Carbon Nanotube-Based Supramolecular Hydrogels. Small 2014, 10, 1387–1393.
- (13) van Gemert, G. M.; Peeters, J. W.; Söntjens, S. H.; Janssen, H. M.; Bosman, A. W. Self-Healing Supramolecular Polymers in Action. *Macromolecular Chemistry and Physics* **2012**, *213*, 234–242.
- (14) Li, X.; Wang, Z.; Li, W.; Sun, J. Superstrong Water-Based Supramolecular Adhesives Derived From Poly (vinyl alcohol)/Poly (acrylic acid) Complexes. *ACS Materials Letters* **2021**, *3*, 875–882.
- (15) Li, X.; Deng, Y.; Lai, J.; Zhao, G.; Dong, S. Tough, Long-Term, Water-Resistant, and Underwater Adhesion of Low-Molecular-Weight Supramolecular Adhesives. *Journal of the American Chemical Society* **2020**, *142*, 5371–5379.
- (16) Li, J.; Luo, S.; Li, F.; Dong, S. Supramolecular Polymeric Pressure-Sensitive Adhesive That Can Be Directly Operated at Low Temperatures. *ACS Applied Materials & Interfaces* **2022**, *14*, 27476–27483.
- (17) Lee, B. P.; Messersmith, P. B.; Israelachvili, J. N.; Waite, J. H. Mussel-Inspired Adhesives and Coatings. *Annual Review of Materials Research* **2011**, *41*, 99–132.
- (18) Hofman, A. H.; van Hees, I. A.; Yang, J.; Kamperman, M. Bioinspired Underwater Adhesives by Using the Supramolecular Toolbox. *Advanced Materials* **2018**, *30*, 1704640.

- (19) Cheng, S.; Zhang, M.; Dixit, N.; Moore, R. B.; Long, T. E. Nucleobase Self-Assembly in Supramolecular Adhesives. *Macromolecules* **2012**, *45*, 805–812.
- (20) Yamauchi, K.; Lizotte, J. R.; Long, T. E. Thermoreversible Poly (alkyl acrylates) Consisting of Self-Complementary Multiple Hydrogen Bonding. *Macromolecules* 2003, 36, 1083–1088.
- (21) Ji, X.; Ahmed, M.; Long, L.; Khashab, N. M.; Huang, F.; Sessler, J. L. Adhesive Supramolecular Polymeric Materials Constructed From Macrocycle-Based Host-Guest Interactions. Chemical Society Reviews 2019, 48, 2682–2697.
- (22) Zhang, Q.; Shi, C.-Y.; Qu, D.-H.; Long, Y.-T.; Feringa, B. L.; Tian, H. Exploring a Naturally Tailored Small Molecule for Stretchable, Self-Healing, and Adhesive Supramolecular Polymers. *Science Advances* **2018**, *4*, eaat8192.
- (23) Endo, K.; Yamanaka, T. Copolymerization of Lipoic Acid With 1, 2-Dithiane and Characterization of the Copolymer as an Interlocked Cyclic Polymer. *Macromolecules* 2006, 39, 4038–4043.
- (24) Kisanuki, A.; Kimpara, Y.; Oikado, Y.; Kado, N.; Matsumoto, M.; Endo, K. Ring-Opening Polymerization of Lipoic Acid and Characterization of the Polymer. *Journal of Polymer Science Part A: Polymer Chemistry* 2010, 48, 5247–5253.
- (25) Zhang, X.; Waymouth, R. M. 1,2-Dithiolane-Derived Dynamic, Covalent Materials: Cooperative Self-Assembly and Reversible Cross-Linking. *Journal of the American Chemical Society* 2017, 139, 3822–3833.
- (26) Shi, C.-Y.; Zhang, Q.; Wang, B.-S.; Chen, M.; Qu, D.-H. Intrinsically Photopolymerizable Dynamic Polymers Derived From a Natural Small Molecule. *ACS Applied Materials & Interfaces* **2021**, *13*, 44860–44867.

- (27) Shi, C.-Y.; He, D.-D.; Zhang, Q.; Tong, F.; Shi, Z.-T.; Tian, H.; Qu, D.-H. Robust and Dynamic Underwater Adhesives Enabled by Catechol-Functionalized Poly (disulfides) Network. *National Science Review* **2022**, nwac139.
- (28) Deng, Y.; Zhang, Q.; Shi, C.; Toyoda, R.; Qu, D.-H.; Tian, H.; Feringa, B. L. Acylhydrazine-Based Reticular Hydrogen Bonds Enable Robust, Tough, and Dynamic Supramolecular Materials. *Science Advances* **2022**, *8*, eabk3286.
- (29) Zhang, Q.; Deng, Y.-X.; Luo, H.-X.; Shi, C.-Y.; Geise, G. M.; Feringa, B. L.; Tian, H.; Qu, D.-H. Assembling a Natural Small Molecule Into a Supramolecular Network With High Structural Order and Dynamic Functions. *Journal of the American Chemical* Society 2019, 141, 12804–12814.
- (30) Chung, W. J. et al. The Use of Elemental Sulfur as an Alternative Feedstock for Polymeric Materials. *Nature Chemistry* **2013**, *5*, 518–524.
- (31) Deng, Y.; Zhang, Q.; Feringa, B. L.; Tian, H.; Qu, D.-H. Toughening a Self-Healable Supramolecular Polymer by Ionic Cluster-Enhanced Iron-Carboxylate Complexes. *Angewandte Chemie* **2020**, *132*, 5316–5321.
- (32) Liu, Y.; Jia, Y.; Wu, Q.; Moore, J. S. Architecture-Controlled Ring-Opening Polymerization for Dynamic Covalent Poly (disulfide) s. *Journal of the American Chemical Society* **2019**, *141*, 17075–17080.
- (33) Wang, B.-S.; Zhang, Q.; Wang, Z.-Q.; Shi, C.-Y.; Gong, X.-Q.; Tian, H.; Qu, D.-H. Acid-catalyzed Disulfide-mediated Reversible Polymerization for Recyclable Dynamic Covalent Materials. *Angewandte Chemie* **2023**, e202215329.
- (34) Harada, A.; Li, J.; Kamachi, M. The Molecular Necklace: A Rotaxane Containing Many Threaded α -Cyclodextrins. *Nature* **1992**, *356*, 325–327.

- (35) Liu, C.; Mayumi, K.; Hayashi, K.; Jiang, L.; Yokoyama, H.; Ito, K. Direct Observation of Large Deformation and Fracture Behavior at the Crack Tip of Slide-Ring Gel. *Journal of the Electrochemical Society* **2019**, *166*, B3143.
- (36) Vernerey, F. J.; Lamont, S. Transient Mechanics of Slide-Ring Networks: A Continuum Model. *Journal of the Mechanics and Physics of Solids* **2021**, *146*, 104212.
- (37) Nakahata, M.; Mori, S.; Takashima, Y.; Yamaguchi, H.; Harada, A. Self-healing Materials Formed by Cross-Linked Polyrotaxanes With Reversible Bonds. *Chem* **2016**, *1*, 766–775.
- (38) Kobayashi, Y.; Zheng, Y.; Takashima, Y.; Yamaguchi, H.; Harada, A. Physical and Adhesion Properties of Supramolecular Hydrogels Cross-Linked by Movable Cross-Linking Molecule and Host-Guest Interactions. Chemistry Letters 2018, 47, 1387–1390.
- (39) Dikshit, K.; Bruns, C. J. Post-Synthesis Modification of Slide-Ring Gels for Thermal and Mechanical Reconfiguration. *Soft Matter* **2021**, *17*, 5248–5257.
- (40) Ohtsuka, K.; Zhao, C. Properties of Bismaleimide Resin Modified With Polyrotaxane as a Stress Relaxation Material. *Polymer International* **2018**, *67*, 1112–1117.
- (41) Mikami, R.; Arisaka, Y.; Hakariya, M.; Iwata, T.; Yui, N. Improved Epithelial Cell-Cell Adhesion Using Molecular Mobility of Supramolecular Surfaces. *Biomaterials Science* 2021, 9, 7151–7158.
- (42) Kang, T. W.; Tamura, A.; Arisaka, Y.; Yui, N. Thin-Layer Photodegradable Polyrotaxane Gel-Immobilized Surfaces for Photoregulation of Surface Properties and Cell Adhesiveness. *Journal of Applied Polymer Science* **2022**, *139*.
- (43) Choi, S.; Kwon, T.-w.; Coskun, A.; Choi, J. W. Highly Elastic Binders Integrating Polyrotaxanes for Silicon Microparticle Anodes in Lithium Ion Batteries. *Science* **2017**, 357, 279–283.

- (44) Yoo, D.-J.; Elabd, A.; Choi, S.; Cho, Y.; Kim, J.; Lee, S. J.; Choi, S. H.; Kwon, T.-w.; Char, K.; Kim, K. J.; Coskun, A.; Choi, J. W. Highly elastic polyrotaxane binders for mechanically stable lithium hosts in lithium-metal batteries. *Advanced Materials* 2019, 31, 1901645.
- (45) Cho, Y.; Kim, J.; Elabd, A.; Choi, S.; Park, K.; Kwon, T.-w.; Lee, J.; Char, K.; Coskun, A.; Choi, J. W. A Pyrene–Poly(acrylic acid)–Polyrotaxane Supramolecular Binder Network for High-Performance Silicon Negative Electrodes. Advanced Materials 2019, 31, 1905048.
- (46) Yi, M.-B.; Lee, T.-H.; Han, G.-Y.; Kim, H.; Kim, H.-J.; Kim, Y.; Ryou, H.-S.; Jin, D.-U. Movable Cross-linking in Adhesives: Superior Stretching and Adhesion Properties *via* a Supramolecular Sliding Effect. *ACS Applied Polymer Materials* **2021**, *3*, 2678–2686.
- (47) Hashidzume, A.; Yamaguchi, H.; Harada, A. Cyclodextrin-Based Rotaxanes: From Rotaxanes to Polyrotaxanes and Further to Functional Materials. *European Journal of Organic Chemistry* **2019**, *2019*, 3344–3357.
- (48) Araki, J.; Ito, K. New Solvent for Polyrotaxane. I. Dimethylacetamide/Lithium Chloride (DMAc/LiCl) System for Modification of Polyrotaxane. *Journal of Polymer Science Part A: Polymer Chemistry* **2005**, *44*, 532–538.
- (49) Samitsu, S.; Araki, J.; Kataoka, T.; Ito, K. New Solvent for Polyrotaxane. II. Dissolution Behavior of Polyrotaxane in Ionic Liquids and Preparation of Ionic Liquid-Containing Slide-Ring Gels. *Journal of Polymer Science B: Polymer Physics* 2006, 44, 1985–1994.
- (50) Rusa, C. C.; Bullions, T. A.; Fox, J.; Porbeni, F. E.; Wang, X.; Tonelli, A. E. Inclusion Compound Formation With a New Columnar Cyclodextrin Host. *Langmuir* **2002**, *18*, 10016–10023.

- (51) Specogna, E.; Li, K. W.; Djabourov, M.; Carn, F.; Bouchemal, K. Dehydration, Dissolution, and Melting of Cyclodextrin Crystals. *The Journal of Physical Chemistry B* **2015**, *119*, 1433–1442.
- (52) Sakai, Y.; Ueda, K.; Katsuyama, N.; Shimizu, K.; Sato, S.; Kuroiwa, J.; Araki, J.; Teramoto, A.; Abe, K.; Yokoyama, H.; Ito, K. Fabrication and Structural Analysis of Polyrotaxane Fibers and Films. *Journal of Condensed Matter Physics* 2011, 23, 284108.
- (53) Okumura, Y.; Ito, K. The Polyrotaxane Gel: A Topological Gel by Figure-of-Eight Cross-links. *Advanced Materials* **2001**, *13*, 485–487.
- (54) Kato, K.; Mizusawa, T.; Yokoyama, H.; Ito, K. Polyrotaxane Glass: Peculiar Mechanics Attributable to the Isolated Dynamics of Different Components. The Journal of Physical Chemistry Letters 2015, 6, 4043–4048.
- (55) Feldstein, M. M.; Siegel, R. A. Molecular and Nanoscale Factors Governing Pressure-Sensitive Adhesion Strength of Viscoelastic Polymers. *Journal of Polymer Science Part* B: Polymer Physics 2012, 50, 739–772.
- (56) Pizzi, A. Recent Developments in Eco-Efficient Bio-Based Adhesives for Wood Bonding: Opportunities and Issues. *Journal of Adhesion Science and Technology* 2006, 20, 829–846.
- (57) Heinrich, L. A. Future Opportunities for Bio-Based Adhesives—Advantages Beyond Renewability. *Green Chemistry* **2019**, *21*, 1866–1888.
- (58) Antov, P.; Savov, V.; Neykov, N. Sustainable Bio-Based Adhesives for Eco-Friendly Wood Composites. A Review. *Wood Research* **2020**, *65*, 51–62.
- (59) Shinohara, Y.; Kayashima, K.; Okumura, Y.; Zhao, C.; Ito, K.; Amemiya, Y. Small-

- Angle X-Ray Scattering Study of the Pulley Effect of Slide-Ring Gels. *Macromolecules* **2006**, *39*, 7386–7391.
- (60) Karino, T.; Shibayama, M.; Okumura, Y.; Ito, K. SANS Study on Pulley Effect of Slide-Ring Gel. *Physica B: Condensed Matter* **2006**, *385-386*, 807–809.
- (61) Trentin, M.; Carofiglio, T.; Fornasier, R.; Tonellato, U. Capillary Zone Electrophoresis Study of Cyclodextrin–Lipoic Acid Host-Guest Interaction. *Electrophoresis* 2002, 23, 4117–4122.
- (62) Rekharsky, M. V.; Inoue, Y. Complexation Thermodynamics of Cyclodextrins. *Chemical Reviews* **1998**, *98*, 1875–1918.
- (63) Araki, J.; Zhao, C.; Ito, K. Efficient Production of Polyrotaxanes from α-Cyclodextrin and Poly(ethylene glycol). Macromolecules 2005, 38, 7524–7527.
- (64) Nordstrand, K.; Åslund, F.; Meunier, S.; Holmgren, A.; Otting, G.; Berndt, K. D. Direct NMR Observation of the Cys-14 Thiol Proton of Reduced Escherichia coli Glutaredoxin-3 Supports the Presence of an Active Site Thiol-Thiolate Hydrogen Bond. FEBS Letters 1999, 449, 196–200.
- (65) Darby, D. R.; Lai, E.; Holten-Andersen, N.; Pham, J. T. Interfacial Adhesion of Fully Transient, Mussel-Inspired Hydrogels with Different Network Crosslink Modalities. Advanced Materials Interfaces 2021, 8, 2100319.
- (66) Darby, D. R.; Cai, Z.; Mason, C. R.; Pham, J. T. Modulus and Adhesion of Sylgard 184, Solaris, and Ecoflex 00-30 Silicone Elastomers With Varied Mixing Ratios. *Journal* of Applied Polymer Science 2022, 139, e52412.
- (67) Ma, J.; Hu, Z.; Wang, W.; Wang, X.; Wu, Q.; Yuan, Z. pH-Sensitive Reversible Programmed Targeting Strategy by the Self-Assembly/Disassembly of Gold Nanoparticles.

 ACS Applied Materials & Interfaces 2017, 9, 16767–16777.

- (68) Yang, W.; Zou, Y.; Meng, F.; Zhang, J.; Cheng, R.; Deng, C.; Zhong, Z. Efficient and Targeted Suppression of Human Lung Tumor Xenografts in Mice With Methotrexate Sodium Encapsulated in All-Function-in-One Chimeric Polymersomes. *Advanced Materials* **2016**, *28*, 8234–8239.
- (69) Takahashi, K.; Oda, R.; Inaba, K.; Kishimoto, K. Scaling Effect on the Detachment of Pressure-Sensitive Adhesives Through Fibrillation Characterized by a Probe-Tack Test. Soft Matter 2020, 16, 6493–6500.
- (70) Sowa, D.; Czech, Z.; Byczyński, Ł. Peel Adhesion of Acrylic Pressure-Sensitive Adhesives on Selected Substrates versus Their Surface Energies. International Journal of Adhesion and Adhesives 2014, 49, 38–43.
- (71) Kowalski, A.; Czech, Z.; Byczyński, Ł. How Does the Surface Free Energy Influence the Tack of Acrylic Pressure-Sensitive Adhesives (PSAs)? Journal of Coatings Technology and Research 2013, 10, 879–885.
- (72) Doi, M.; Edwards, S. F. *The Theory of Polymer Dynamics*; Oxford University Press: Oxford, 1988.
- (73) Creton, C. Pressure-Sensitive Adhesives: An Introductory Course. MRS Bulletin 2003, 28, 434–439.
- (74) Williams, G.; Watts, D. C. Non-Symmetrical Dielectric Relaxation Behaviour Arising From a Simple Empirical Decay Function. Transactions of the Faraday Society 1970, 66, 80–85.
- (75) Gotze, W.; Sjogren, L. Relaxation Processes in Supercooled Liquids. *Reports on Progress in Physics* **1992**, *55*, 241.
- (76) Goodwin, A. A.; Simon, G. P. Dynamic Mechanical Relaxation Behaviour of Poly (ether ether ketone)/Poly (etherimide) Blends. *Polymer* **1997**, *38*, 2363–2370.

- (77) Liu, J.; Lin, P.; Li, X.; Wang, S.-Q. Nonlinear Stress Relaxation Behavior of Ductile Polymer Glasses From Large Extension and Compression. *Polymer* **2015**, *81*, 129–139.
- (78) Tang, S.; Wang, M.; Olsen, B. D. Anomalous self-diffusion and sticky Rouse dynamics in associative protein hydrogels. *Journal of the American Chemical Society* 2015, 137, 3946–3957.
- (79) Bandyopadhyay, R.; Mohan, P. H.; Joshi, Y. M. Stress Relaxation in Aging Soft Colloidal Glasses. *Soft Matter* **2010**, *6*, 1462–1466.
- (80) López-Suevos, F.; Frazier, C. E. Wood-Adhesive Interactions in a PVAc Latex. *Holz-forschung* **2008**, *62*, 468–471.
- (81) LaPlante, G.; Lee-Sullivan, P. Moisture Effects on FM300 Structural Film Adhesive: Stress Relaxation, Fracture Toughness, and Dynamic Mechanical Analysis. *Journal of Applied Polymer Science* **2005**, *95*, 1285–1294.
- (82) Jose, J.; Swaminathan, N. Response of Adhesive Polymer Interfaces to Repeated Mechanical Loading and the Spatial Variation of Diffusion Coefficient and Stresses in a Deforming Polymer Film. *Physical Chemistry Chemical Physics* **2019**, *21*, 11266–11283.
- (83) Creton, C.; Leibler, L. How Does Tack Depend on Time of Contact and Contact Pressure? *Journal of Polymer Science Part B: Polymer Physics* **1996**, *34*, 545–554.
- (84) Novikov, M. B.; Borodulina, T. A.; Kotomin, S. V.; Kulichikhin, V. G.; Feldstein, M. M. Relaxation Properties of Pressure-Sensitive Adhesives Upon Withdrawal of Bonding Pressure. The Journal of Adhesion 2005, 81, 77–107.
- (85) Johnson, P. M.; Stafford, C. M. Effect of Interfacial Adhesion on Viscoelastic Relaxation Processes in Thin Polymer Film Indentation. ACS Applied Materials & Interfaces 2010, 2, 2108–2115.

- (86) Gunawan, M.; Wong, E.-H.; Mhaisalkar, S. G.; Davila, L. T.; Hong, Y.; Caers, J.; Tsai, T.-K. Characterization and Modeling of Static and Cyclic Relaxation in Nonconductive Adhesives. *Journal of Electronic Materials* **2004**, *33*, 1041–1047.
- (87) Brown, K.; Hooker, J. C.; Creton, C. Micromechanisms of Tack of Soft Adhesives Based on Styrenic Block Copolymers. *Macromolecular Materials and Engineering* **2002**, *287*, 163–179.
- (88) Yazdani-Ahmadabadi, H.; Rastegar, S.; Ranjbar, Z. A Modified de Gennes's Trumpet Model for the Prediction of Practical Adhesion of Dynamically and Structurally Heterogeneous Polymeric Networks on Solid Surfaces. RSC Advances 2015, 5, 49400–49407.
- (89) Chang, E. P. Viscoelastic Properties of Pressure-Sensitive Adhesives. *The Journal of Adhesion* **1997**, *60*, 233–248.
- (90) Taghizadeh, S. M.; Ghasemi, D. Rheological and Adhesion Properties of Acrylic Pressure-Sensitive Adhesives. *Journal of Applied Polymer Science* **2011**, *120*, 411–418.
- (91) Dahlquist, C. A. Pressure-Sensitive Adhesives. *Treatise on Adhesion and Adhesives* **1969**, 2, 219–260.
- (92) Callies, X.; Fonteneau, C.; Pensec, S.; Bouteiller, L.; Ducouret, G.; Creton, C. Adhesion and Non-Linear Rheology of Adhesives With Supramolecular Crosslinking Points. *Soft Matter* **2016**, *12*, 7174–7185.
- (93) Du, J.; Lindeman, D. D.; Yarusso, D. J. Modeling the Peel performance of Pressure-Sensitive Adhesives. *The Journal of Adhesion* **2004**, *80*, 601–612.
- (94) Ikuta, N.; Sugiyama, H.; Shimosegawa, H.; Nakane, R.; Ishida, Y.; Uekaji, Y.; Nakata, D.; Pallauf, K.; Rimbach, G.; Terao, K., et al. Analysis of the Enhanced Stability of R (+)-Alpha Lipoic Acid by the Complex Formation With Cyclodextrins. International Journal of Molecular Sciences 2013, 14, 3639–3655.

- (95) Le, T. M. N.; Dang, L. V.; Washizu, H. Structural Order of Water Molecules Around Polyrotaxane Including PEG, α-Cyclodextrin, and α-Lipoic Acid Linker on Gold Surface by Molecular Dynamics Simulations. Physical Chemistry Chemical Physics 2022, 24, 2176–2184.
- (96) Rusa, C. C.; Tonelli, A. E. Polymer/Polymer Inclusion Compounds as a Novel Approach to Obtaining a PLLA/PCL Intimately Compatible Blend. *Macromolecules* **2000**, *33*, 5321–5324.
- (97) Huh, K. M.; Ooya, T.; Sasaki, S.; Yui, N. Polymer Inclusion Complex Consisting of Poly (ε -lysine) and α -Cyclodextrin. *Macromolecules* **2001**, 34, 2402–2404.
- (98) Rusa, C. C.; Bridges, C.; Ha, S.-W.; Tonelli, A. E. Conformational Changes Induced in *Bombyx mori* Silk Fibroin by Cyclodextrin Inclusion Complexation. *Macromolecules* **2005**, *38*, 5640–5646.